

# Further Insight into the DNA Recognition Mechanism of Trabectedin from the Differential Affinity of Its Demethylated Analogue Ecteinascidin ET729 for the Triplet DNA Binding Site CGA

Esther Marco,<sup>†,‡</sup> Marie-Hélène David-Cordonnier,<sup>§</sup> Christian Bailly,<sup>§</sup> Carmen Cuevas,<sup>#</sup> and Federico Gago\*<sup>†</sup>

Departamento de Farmacología, Universidad de Alcalá, E-28871 Alcalá de Henares, Madrid, Spain, INSERM U-524 and Laboratoire de Pharmacologie Antitumorale du Centre Oscar Lambret, IRCL, Place de Verdun, F-59045 Lille, France, and PharmaMar S. A., Avda. de los Reyes, 1 Polígono Industrial La Mina, E-28770 Colmenar Viejo, Madrid, Spain

Received May 30, 2006

Trabectedin and its N12-demethylated analogue ET729 bind covalently to the central guanine of selected DNA triplets. Although both drugs equally target several sites, including AGA, we show that covalent modification of CGA is only achieved by ET729. By means of molecular dynamics simulations of the pre-covalent complexes, we explain in atomic detail how such a simple structural modification brings about this notable change in the DNA-binding selectivity profiles of these two drugs.

## Introduction

The potent anticancer agent trabectedin (Yondelis), presently in phase II/III clinical trials,<sup>1</sup> was originally isolated with very low yields from the marine tunicate *Ecteinascidia turbinata*<sup>2,3</sup> but is now obtained in multigram quantities through chemical modification of microbially produced cyanosafrafrin B.<sup>4</sup> Trabectedin consists of a polycyclic skeleton composed of three fused tetrahydroisoquinoline rings (Figure 1A) and binds to guanines in the minor groove of DNA by virtue of its reactive 21-carbinolamine (hemiaminal) group.<sup>5</sup> The binding site covers three base pairs, and the exocyclic amino group of the guanine in the middle of the triplet is necessary for the covalent binding of the drug.<sup>6</sup> The resulting adduct is then stabilized by the hydrogen bonds established between the N12 in subunit A and a hydrogen-bond acceptor atom (O2 or N3) located 5' to the modified guanine in the opposite strand and between the inner geminal diether (methylenedioxy) oxygen in subunit B and the amino group of another guanine located 3' to the modified guanine in the same or the opposite strand. Sequence selectivity was then proposed to operate predominantly through a set of hydrogen-bonding rules<sup>7</sup> such that preferred target triplets are 5'-RGC and 5'-YGG, where R and Y stand for purine and pyrimidine, respectively, and the underlined base is the guanine whose exocyclic amino group effects the nucleophilic attack at C21 (Figure 1B). Examples of favored and well-studied triplets are TGG, CGG, AGC, and GGC, all of which provide an optimal arrangement of hydrogen-bonding donor/acceptor atoms on both DNA strands that is believed to properly orientate the drug in the minor groove and catalyze dehydration of the carbinolamine and generation of the reactive iminium intermediate.<sup>5,8</sup>

On the basis of this scheme, 5'-NG(A/T) sequences were predicted to be disfavored because they lack a hydrogen bond donor on the 3' side of the central guanine.<sup>5</sup> However, later studies demonstrated similar reaction of trabectedin with AGC

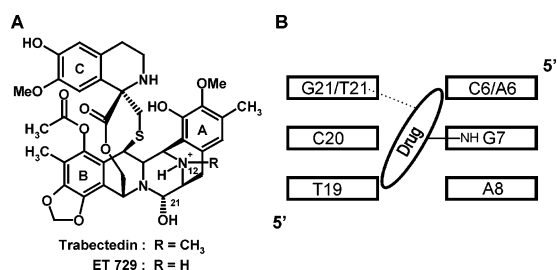


**Figure 1.** (A) Chemical structures of trabectedin and ET729. (B) Schematic of the binding mode of these drugs to a central CGA or AGA triplet in the DNA 13-mers studied showing the base-pair numbering scheme, the covalent bond (line), and the hydrogen bond (dotted line).

and AGT triplets (although the rate of reversibility was found to be greatly enhanced in the case of the AGT adduct)<sup>9</sup> and comparable binding of trabectedin to GGG and AGA triplets.<sup>10</sup> This means that, at least when embedded in a suitable sequence context, several 5'-RG(A/T) sequences can also be targeted by this drug. Nonetheless, the CGA triplet has been consistently shown to be disfavored by trabectedin, which is in agreement with the importance attached to the 2-amino group in the minor groove on the 3' side of the central guanine.<sup>6,10,11</sup>

Strikingly, when we studied the sequence binding preferences of the N12-demethylated analogue of trabectedin, ET729 (Figure 1A), we found that this compound not only binds to AGA sites as well but is also capable of reacting with the central guanine in a CGA triplet. This is an interesting observation by itself because ET729 has been shown to be one of the main metabolites of trabectedin in humans,<sup>12</sup> and it is therefore possible that ET729 could contribute to some aspects of the activity of the clinical candidate, but it can also help clarify mechanistic aspects of the bonding reaction. Since both ecteinascidins share the same hydrogen-bonding functionalities, we have tried to gain insight into the additional factors responsible for the distinct selectivity profiles of these two compounds by studying in atomic detail the feasibility of achieving the geometries required to activate dehydration of the carbinolamine prior to the nucleophilic attack that leads to covalent bond formation. To this end, we have modeled and simulated using molecular dynamics (MD) the pre-covalent binding complexes of trabectedin and ET729 with three double-stranded oligo-

\* To whom correspondence should be addressed. Telephone: +34-918 854 514. Fax: +34-918 854 591. E-mail: federico.gago@uah.es.

<sup>†</sup> Universidad de Alcalá.

<sup>‡</sup> Present address: INSERM U-531, Institut Louis Bugnard, Avenue Jean Poulhès BP 84225, 31432 Toulouse Cedex 4, France.

<sup>§</sup> INSERM U-524 and Laboratoire de Pharmacologie Antitumorale du Centre Oscar Lambret.

<sup>#</sup> PharmaMar S. A.

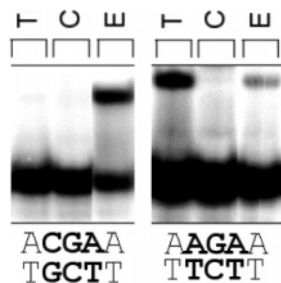


**Figure 2.** Mobility shift in polyacrylamide gels of CGA- and AGA-containing oligonucleotides (C) brought about by binding of trabectedin (T) or ET729 (E).

nucleotides containing the sequences 5'-CAATACGAATAAG, 5'-CAATAAGAATAAG, and 5'-CAATACGGATAAG. Simulations of these oligonucleotides in the free state were also run under identical conditions for control and comparison purposes.

### Results and Discussion

The results of a representative band-shift assay are shown in Figure 2. By comparison of the intensities of the bands corresponding to the drug–DNA complexes to those of the free DNA, it can be clearly seen that both drugs react with the AGA sequence and also that the CGA-containing oligonucleotide is targeted by ET729 but not by trabectedin.

In the simulated precovalent complexes of ET729 or trabectedin with the AGA- and CGG-containing oligonucleotides, the geometry required for attack was rapidly attained (Figure 3), and this was similar to that previously reported for AGC.<sup>11</sup> This finding is consistent with the fact that both drugs are able to react with these triplet sites. The protonated N12 of both drugs remained hydrogen-bonded to the O2 acceptor atom of T21 in the AGA triplet and to N3 of G21 in the case of the CGG triplet, whereas the carbinol OH was seen to act both as a hydrogen

bond donor to O2 of C20 and as a hydrogen bond acceptor from N2(G7) (Table 1). This geometry lends strong support to the proposal that the former hydrogen bond weakens the N12–H12 covalent bond, thus facilitating transfer of H12 to the carbinol OH, whereas the second hydrogen bond debilitates the C21–OH bond, thus favoring the exit of the water molecule.<sup>5</sup> Opening of the G7:C20 base pair, which was larger in the AGA relative to the CGG precovalent complexes, disrupted the O6(G7)–N4(C20) and N1(G7)–N3(C20) hydrogen bonds, whereas a new hydrogen bond was formed between N2(G7) and N3(C20). The OH of subunit C, which was far from any phosphate backbone oxygen in the initial structure, approached the O1P of the phosphate linking T10–T11 within hydrogen-bonding distance. This stable hydrogen bond helped the drug to get fully inserted within the minor groove and brought the methylenedioxy group of subunit B close to H2(A8) in a manner similar to that found in the covalent complexes.<sup>7,11</sup> In the case of both CGG complexes, an additional intermolecular hydrogen bond between the methylenedioxy oxygen facing the minor groove and the amino group of G8 favored a deeper penetration of subunit B into the minor groove.

In contrast, in the case of the CGA triplet, trabectedin was not stabilized by any of these key intermolecular interactions because the required hydrogen-bonding distances were too long (Table 1), and a proper attack orientation could not be adopted for this drug. Our hypothesis that this is mostly due to the steric clash between the N12 methyl of trabectedin and the exocyclic amino group of G21 was supported by our finding that ET729, which lacks this methyl group, was able to achieve, and maintain for the whole length of the simulation, the optimal geometry with the CGA triplet (Figure 4), as described above for AGA and CGG. Since this steric clash is also present in the CGG precovalent complex, the evidence suggests that this negative effect for trabectedin can be overridden by the stabilizing

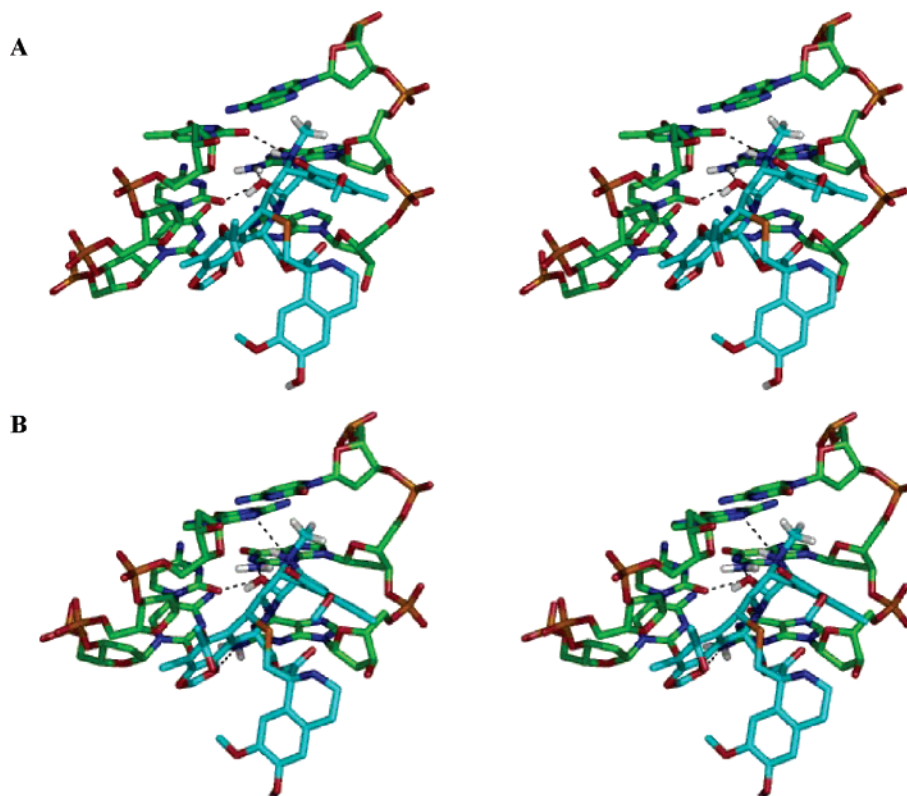


**Figure 3.** Stereoviews showing a detail of the precovalent complexes between trabectedin (C atoms in cyan) and (A) the AGA- and (B) CGG-containing oligo-nucleotides (C atoms in green). Crucial hydrogen bonds are displayed as dotted lines.

**Table 1.** Relevant Intermolecular Distances (Å) and Angles (deg) between Hydrogen-Bonding Donor and Acceptor Atoms in the Six Precovalent Complexes Studied

	AGA			CGA			CGG					
	trabectedin		ET729	trabectedin		ET729	trabectedin		ET729			
	distance	angle	distance	angle	distance	angle	distance	angle				
OH–O2(C20) <sup>b</sup>	2.7 ± 0.1	153.1 ± 9.9	2.7 ± 0.1	155 ± 10.4	3.0 ± 0.3	94.4 ± 47.8	2.7 ± 0.1	153.7 ± 11.7	2.8 ± 0.2	149.2 ± 14.3	2.8 ± 0.3	146.5 ± 16.5
OH–N2(G7)	2.9 ± 0.1	159.7 ± 10.2	3.0 ± 0.2	154.7 ± 10.9	4.4 ± 0.4	11.5 ± 0.4	3.0 ± 0.3	100.1 ± 17.0	3.0 ± 0.2	109.6 ± 15.1	2.9 ± 0.1	111.6 ± 14.9
N12–O2(T21)	2.8 ± 0.1	142.8 ± 8.7	2.8 ± 0.1	151.4 ± 10.2								
N12–N3(G21)					4.1 ± 0.4	108.4 ± 11.5	2.9 ± 0.1	150.9 ± 10	3.3 ± 0.2	138.9 ± 10.1	2.9 ± 0.1	150.9 ± 10
OM–H2(A8)	3.7 ± 0.5		3.9 ± 0.4				3.5 ± 0.4 <sup>c</sup>		3.5 ± 0.4 <sup>c</sup>			
OM–N2(G8)					7.6 ± 1.1	67.5 ± 21.2	3.2 ± 1.3	148.7 ± 29.2	3.1 ± 0.2	133.7 ± 13.5	3.1 ± 0.2	135.7 ± 12.7
OHC–O1P(T10)	2.8 ± 0.4	155.4 ± 14.0	3.0 ± 0.6	149.0 ± 23.2			2.7 ± 0.2	157.6 ± 10.8	2.7 ± 0.2	157.6 ± 10.8	2.7 ± 0.3	155.7 ± 16.4

<sup>a</sup> Average distance ± standard deviation over the 2 ns of the simulation. <sup>b</sup> OH is the carbinol hydroxyl oxygen and OHC is the phenolic oxygen from subunit C. The methylenedioxy oxygen, OM, is also included for comparison (see text for details). <sup>c</sup> Average distance ± standard deviation over the last 1500 ps of the simulation.

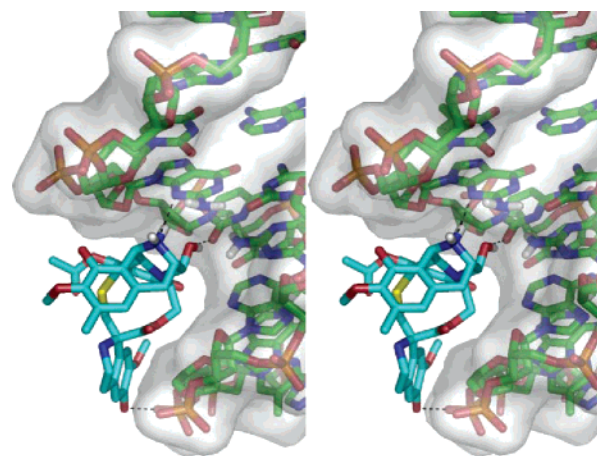


**Figure 4.** Stereoview showing the precovalent ET729:CGA complex in which a semitransparent solvent-accessible surface envelops the DNA atoms. Drug and DNA carbon atoms have been colored cyan and green, respectively. Only hydrogens attached to N12 and O21 of ET729 and the amino groups of G7 and G21 are shown. Crucial hydrogen bonds are displayed as dotted lines. The N12 proton that is not involved in hydrogen bonding is replaced with a methyl group in trabectedin (cf. Figure 3).

hydrogen bond between the inner methylenedioxy oxygen and the amino group that is present in G8 (CGG) but missing in A8 (CGA).

When we compared the DNA base-step geometries of the central CGG, AGA, and CGA triplets in the precovalent complexes and in the free oligonucleotides, distinctive changes were observed in roll, slide, and shift parameters (Table 2). The intrinsic positive roll of the C6/G7 step and the systematic increases in roll brought about by drug binding are consistent with previous reports.<sup>11,13,14</sup> In addition, the overall null shift for C6/G7 and G7/A8 steps in the free CGA oligonucleotide gave rise, upon binding of ET729, to positive and negative values, respectively, that were clearly anticorrelated during the MD trajectory once the drug became fully inserted into the minor groove (Supporting Information, Figure S1). It was at this stage that the gap between the methylenedioxy oxygen and H2(A8) was shortened and the separation between the carbinol OH and N2(G7) fell within hydrogen-bonding distance (Supporting Information, Figure S2). A similar situation was detected in the case of CGG and AGA triplets, and an anticorrelation was also found between positive shift for C6/G7 and A6/G7 steps and negative shift for G7/G8 and G7/A8 steps (Table 2). This anticorrelation appeared to be strictly dependent on the existence of the carbinol OH–O2(C20) hydrogen bond because it was temporarily lost when this direct interaction was disrupted (Supporting Information, Figure S3). The negative shift values for C6/G7 and A6/G7 revealed the displacement of the C6: G21 and A6:T21 base pairs toward the minor groove as a consequence of the hydrogen-bonding interaction between the protonated N12 of each drug and N3(G21) or O2(T21) DNA acceptor atoms, whereas the positive shift values for both G7/A8 steps reflected the displacement of the G7:C20 base pair toward the major groove as a consequence of the full penetration of the bulky drug into the minor groove. This was accompanied by widening of the minor groove with respect to the free oligonucleotide, which was apparent in all the complexes, with the exception of CGA:trabectedin (Supporting Information, Table S1).

## Conclusions

Our work demonstrates the need to expand the repertoire of triplet sites that trabectedin can target and provides an explana-

**Table 2.** Comparison of Local Helix Parameters<sup>a</sup> for the Central Three Base Pair Steps in the Free Oligonucleotides and in the Precovalent Binding Complexes of Trabectedin and ET729

	shift (Å)		slide (Å)		roll (deg)	
	A6/G7	G7/A8	A6/G7	G7/A8	A6/G7	G7/A8
free AGA	-0.8 ± 0.7	-0.1 ± 0.5	-1.2 ± 0.5	-1.2 ± 0.4	1.9 ± 6.0	1.7 ± 5
trabectedin:AGA	1.6 ± 0.4	-1.6 ± 0.5	0.6 ± 0.6	-1.0 ± 0.4	13.3 ± 5.2	11.1 ± 5.4
ET729:AGA	1.9 ± 0.4	-1.6 ± 0.3	0.2 ± 0.4	-0.8 ± 0.4	9.5 ± 4.5	10.1 ± 5.4
	shift (Å)		slide (Å)		roll (deg)	
	C6/G7	G7/A8	C6/G7	G7/A8	C6/G7	G7/A8
free CGA	0.2 ± 1.2	-0.4 ± 0.8	-0.4 ± 1.2	-0.5 ± 0.6	8.0 ± 6.4	1.2 ± 5.7
trabectedin:CGA	0.9 ± 0.4	-1.2 ± 0.5	-1.2 ± 0.5	0.1 ± 4.8	15.0 ± 8.3	-4.3 ± 8.0
ET729:CGA <sup>b</sup>	1.3 ± 0.4	-1.3 ± 0.3	0.6 ± 0.5	-0.2 ± 0.4	16.3 ± 5.5	1.1 ± 5.0
	shift (Å)		slide (Å)		roll (deg)	
	C6/G7	G7/G8	C6/G7	G7/G8	C6/G7	G7/G8
free CGG	-0.1 ± 0.8	-0.2 ± 0.7	-0.3 ± 0.6	-1.3 ± 0.8	3.9 ± 6.1	3.4 ± 5.2
trabectedin:CGG	1.5 ± 0.4	-1.6 ± 0.4	0.2 ± 0.5	-0.6 ± 0.3	22.5 ± 6.7	2.6 ± 7.5
ET729:CGG	1.4 ± 0.4	-1.6 ± 0.4	0.3 ± 0.5	-0.5 ± 0.3	20.1 ± 7.0	-0.4 ± 7.5

<sup>a</sup> Average value ± standard deviation from the whole length of the MD simulation. <sup>b</sup> Average value ± standard deviation obtained from the last 1500 ps of the MD simulation.

tion in atomic detail for the finding that such a simple structural modification as the replacement of a methyl group by a hydrogen brings about a notable change in the DNA-binding selectivity profile of an interesting antitumor agent that is well advanced into clinical trials. The latter observation is potentially interesting for *in vivo* studies because trabectedin has been shown to be N-demethylated to ET729 by human CYP3A4.<sup>12</sup>

The subtle differences in orientation and geometry reported here are sufficient to rationalize the experimental observations regarding AGA and CGA DNA triplets, thus revealing the power of state-of-the-art MD simulations to probe the details of ligand–DNA interactions in the absence of experimental restraints. The fact that CGG triplets provide good binding sites for trabectedin is due to the fact that anchoring of the methylenedioxy group by the amino group present in the minor groove on the 3' side of the triplet determines a subtle change in overall orientation that is enough to counterbalance the steric clash between the methyl group on N12 and the amino group from the base pair on the 5' side.<sup>11</sup> Thus, it is this moiety that plays a crucial role in the discrimination by trabectedin against a G:C base pair on the 5' side of the covalently modified guanine when an A:T base pair is found on the 3' side (e.g., CGA). This interpretation also provides a rationale to the finding that CGT, GGT, and GGA are nonfavored sites for trabectedin binding because the drug is unable to achieve the optimal juxtaposition required to promote its activation.

## Experimental Procedures

Trabectedin and ET729 were synthesized by PharmaMar (Colmenar Viejo, Madrid, Spain) as described previously.<sup>15</sup> For the mobility shift assays, synthetic double-stranded oligonucleotides of sequence 5'-d(ATAATAXXXATAATA)/5'-d(TATTATYYTAT-TAT), in which the central XXX/YYY triplet was AGA/TCT, CGG/CCG, or CGA/TCG, were prepared by mixing the complementary 15-mers at a 1:1 ratio, heating to 75 °C, and slowly cooling to form duplexes, which were then labeled at the 5' end by using  $\gamma$ -[<sup>32</sup>P]-ATP and T4 polynucleotide kinase. Labeled DNA was then purified by electrophoresis on a 10% (w/v) polyacrylamide gel to remove the excess radioactive nucleotide, cut out of the gel, and eluted overnight in 10 mM Tris (pH 8.0), 1 mM EDTA, 100 mM NaCl. Samples were then ethanol-precipitated, and the DNA pellet was dissolved in water. The reaction consisted of incubating 20 000 cpm radiolabeled DNA with the test drug (15  $\mu$ M each) for 1 h at 37 °C in 20  $\mu$ L of binding buffer (10 mM Tris [pH 7.0], 10 mM NaCl). After the addition of 5  $\mu$ L of a 50% glycerol solution, DNA

samples were resolved by electrophoresis under nondenaturing conditions in 10% polyacrylamide gels for about 4 h at 300 V at room temperature in TBE buffer (89 mM Tris base, 89 mM boric acid, 2.5 mM Na<sub>2</sub>EDTA [pH 8.3]). Gels were transferred to Whatman 3MM paper, dried under vacuum at 80 °C, and then analyzed on a Molecular Dynamics 445SI phosphorimager (Molecular Dynamics, Sunnyvale, CA).

**Computational Methods.** The X-ray crystal structure of the 2-propanol disolvate of trabectedin<sup>16</sup> was used for constructing N12-protonated trabectedin and ET729 (Figure 1A). Each molecule was then broken down into three suitable fragments that were used as input for the *ab initio* quantum mechanical program Gaussian 98<sup>17</sup> in order to derive RHF 6-31G\*//3-21G\* RESP charges,<sup>18</sup> and appropriate bonded and nonbonded parameters consistent with the second-generation AMBER force field<sup>19</sup> (parm99) were assigned (Supporting Information). Models of the free oligonucleotides were built using optimized parameters for B-DNA.<sup>20</sup> Each molecular system was neutralized by addition of the appropriate number of sodium ions, placed in positions of negative electrostatic potential, and immersed in a rectangular box of ~4600 TIP3 model water molecules. Each water box extended 8 Å away from any solute atom, and the cutoff distance for the nonbonded interactions was 9 Å. Periodic boundary conditions were used, and electrostatic interactions were represented using the smooth particle-mesh Ewald method with a grid spacing of ~1 Å. The second-generation AMBER force field<sup>21</sup> updated with new DNA parameters for improved sugar pucker phases and helical repeat (parm99) was used. The SHAKE algorithm was applied to all bonds involving hydrogens, and an integration step of 2 fs was used throughout. The simulation protocol was as previously described<sup>11</sup> and made use of the SANDER module in AMBER, version 6.0.<sup>22</sup> The initial structures of the precovalent complexes were obtained by averaging over 1 ns the model-built free 13-mers in the standard B-DNA conformation, which were also simulated under identical conditions during 2 ns for control and comparison purposes. The drugs were oriented to form one hydrogen bond between the protonated N12 and an acceptor atom of the DNA base at position 21 and another one between the carbinol OH and N2(G7). For the results to be unbiased, only subunit A in the initial structure was located within the minor groove whereas subunits B and C protruded out. The CARNAL module in AMBER was used to monitor root-mean-square deviations (rmsd) and interatomic distances, whereas the CURVES program<sup>23</sup> was employed in the analysis of the conformational and helical parameters of the DNA oligonucleotides. The 3D structures and trajectories were visually inspected using the computer graphics program PyMOL.<sup>24</sup>

**Acknowledgment.** During the course of this work E.M. enjoyed a fellowship from Junta de Comunidades de Castilla-La Mancha. This research was supported in part by grants from the Ligue Nationale Contre le Cancer (Comité du Nord) and the Institut de Recherches sur le Cancer de Lille (to C.B.) and from the Spanish CICYT (Grant SAF2003-7219-C02), Pharma-Mar (Colmenar Viejo, Madrid) and the National Foundation for Cancer Research (to F.G.). We thank the University of Alcalá Computing Centre and the CIEMAT (Madrid) for generous allowances of computer time on their SGI servers.

**Supporting Information Available:** The AMBER PREP files written for ET729 and trabectedin, one table showing the minor groove width of the precovalent complexes, and three additional figures displaying the time evolution of the shift parameter for C6/G7 and G7/A8 steps in the ET729:CGA precovalent complex, the time evolution of relevant intermolecular distances in the trabectedin:CGA and ET729:CGA complexes, and the time evolution of relevant geometrical parameters in the trabectedin:AGA precovalent complex. This material is available free of charge via the Internet at <http://pubs.acs.org>.

## References

- van Kesteren, C.; de Vooght, M. M.; López-Lázaro, L.; Mathot, R. A.; Schellens, J. H.; Jimeno, J. M.; Beijnen, J. H. Yondelis (trabectedin, ET-743): the development of an anticancer agent of marine origin. *Anti-Cancer Drugs* **2003**, *14*, 487–502.
- Rinehart, K. L. Antitumor compounds from tunicates. *Curr. Med. Chem.: Anti-Cancer Agents* **2001**, *1*, 257–276.
- Manzanares, I.; Cuevas, C.; García-Nieto, R.; Marco, E.; Gago, F. Advances in the chemistry and pharmacology of ecteinascidins, a promising new class of anticancer agents. *Curr. Med. Chem.: Anti-Cancer Agents* **2001**, *1*, 257–276.
- Cuevas, C.; Pérez, M.; Martín, M. J.; Chicharro, J. L.; Fernández-Rivas, C.; Flores, M.; Francesch, A.; Gallego, P.; Zarzuelo, M.; de la Calle, F.; García, J.; Polanco, C.; Rodríguez, I.; Manzanares, I. Synthesis of ecteinascidin ET-743 and phthalascidin Pt-650 from cyanosafrafrin B. *Org. Lett.* **2000**, *2*, 2545–2548.
- Gago, F.; Hurley, L. H. In *Small Molecule DNA and RNA Binders: From Synthesis to Nucleic Acid Complexes*; Demeunynck, M., Bailly, C., Wilson, W. D., Eds.; Wiley-VCH: Weinheim, Germany, 2002; pp 643–675.
- Pommier, Y.; Kohlhagen, G.; Bailly, C.; Waring, M.; Mazumder, A.; Kohn, K. W. DNA sequence- and structure-selective alkylation of guanine N2 in the DNA minor groove by ecteinascidin 743, a potent antitumor compound from the Caribbean tunicate *Ecteinascidia turbinata*. *Biochemistry* **1996**, *35*, 13303–13309.
- Seaman, F. C.; Hurley, L. H. Molecular basis for the DNA sequence selectivity of ecteinascidin 736 and 743: evidence for the dominant role of direct readout via hydrogen bonding. *J. Am. Chem. Soc.* **1998**, *120*, 13028–13041.
- Moore, B. M., II; Seaman, F. C.; Wheelhouse, R. T.; Hurley, L. H. Mechanism for the catalytic activation of ecteinascidin 743 and its subsequent alkylation of guanine N2. *J. Am. Chem. Soc.* **1998**, *120*, 2490–2491.
- Zewail-Foote, M.; Hurley, L. H. Differential rates of reversibility of ecteinascidin 743–DNA covalent adducts from different sequences lead to migration to favored bonding sites. *J. Am. Chem. Soc.* **2001**, *123*, 6485–6495.
- David-Cordonnier, M.-H.; et al. DNA and non-DNA targets in the mechanism of action of the antitumor drug trabectedin. *Chem. Biol.* **2005**, *12*, 1201–1210.
- García-Nieto, R.; Manzanares, I.; Cuevas, C.; Gago, F. Bending of DNA upon binding of ecteinascidin 743 and phthalascidin 650 studied by unrestrained molecular dynamics simulations. *J. Am. Chem. Soc.* **2000**, *122*, 7172–7182.
- Reid, J. M.; Kuffel, M. J.; Ruben, S. L.; Morales, J. J.; Rinehart, K. L.; Squillace, D. P.; Ames, M. M. Rat and human liver cytochrome P-450 isoform metabolism of ecteinascidin 743 does not predict gender-dependent toxicity in humans. *Clin. Cancer Res.* **2002**, *8*, 2952–2962.
- Marco, E.; García-Nieto, R.; Mendieta, J.; Manzanares, I.; Cuevas, C.; Gago, F. A 3•(ET743)–DNA complex that both resembles an RNA–DNA hybrid and mimics zinc finger-induced DNA structural distortions. *J. Med. Chem.* **2002**, *45*, 871–880.
- Marco, E.; Gago, F. DNA structural similarity in the 2:1 complexes of the antitumor drugs trabectedin (Yondelis) and chromomycin A<sub>3</sub> with an oligonucleotide sequence containing two adjacent TGG binding sites on opposing strands. *Mol. Pharmacol.* **2005**, *68*, 1559–1567.
- Menchaca, R.; Martínez, V.; Rodríguez, A.; Rodríguez, N.; Flores, M.; Gallego, P.; Manzanares, I.; Cuevas, C. Synthesis of natural ecteinascidins (ET-729, ET-745, ET-759B, ET-736, ET-637, ET-594) from cyanosafrafrin B. *J. Org. Chem.* **2003**, *68*, 8859–8866.
- Sainz-Diaz, C. I.; Manzanares, I.; Francesch, A.; García-Ruiz, J. The potent anticancer compound ecteinascidin-743 (ET-743) as its 2-propanol disolvate. *Acta Crystallogr. C* **2003**, *59*, o197–o198.
- Frisch, M. J.; Trucks, G. W.; Schlegel, H. B.; Scuseria, G. E.; Robb, M. A.; Cheeseman, J. R.; Zakrzewski, V. G.; Montgomery, J. A., Jr.; Stratmann, R. E.; Burant, J. C.; Dapprich, S.; Millam, J. M.; Daniels, A. D.; Kudin, K. N.; Strain, M. C.; Farkas, O.; Tomasi, J.; Barone, V.; Cossi, M.; Cammi, R.; Mennucci, B.; Pomelli, C.; Adamo, C.; Clifford, S.; Ochterski, J.; Petersson, G. A.; Ayala, P. Y.; Cui, Q.; Morokuma, K.; Malick, D. K.; Rabuck, A. D.; Raghavachari, K.; Foresman, J. B.; Cioslowski, J.; Ortiz, J. V.; Stefanov, B. B.; Liu, G.; Liashenko, A.; Piskorz, P.; Komaromi, I.; Gomperts, R.; Martin, R. L.; Fox, D. J.; Keith, T.; Al-Laham, M. A.; Peng, C. Y.; Nanayakkara, A.; Gonzalez, C.; Challacombe, M.; Gill, P. M. W.; Johnson, B. G.; Chen, W.; Wong, M. W.; Andres, J. L.; Head-Gordon, M.; Replogle, E. S.; Pople, J. A. *Gaussian 98*, revision A.11.2; Gaussian, Inc.: Pittsburgh, PA, 2001.
- Bayly, C. I.; Cieplak, P.; Cornell, W. D.; Kollman, P. A. A well-behaved electrostatic potential based method using charge restraints for deriving atomic charges: the RESP model. *J. Phys. Chem.* **1993**, *97*, 10269–10280.
- Cornell, W. D.; Cieplak, P.; Bayly, C. I.; Gould, I. R.; Merz, K. M.; Ferguson, D. M.; Spellmeyer, D. C.; Fox, T.; Caldwell, J. W.; Kollman, P. A. A second generation force field for the simulation of proteins, nucleic acids, and organic molecules. *J. Am. Chem. Soc.* **1995**, *117*, 5179–5197.
- Arnott, S.; Hukins, D. W. Optimised parameters for A-DNA and B-DNA. *Biochem. Biophys. Res. Commun.* **1972**, *47*, 1504–1509.
- Cornell, W. D.; Cieplak, P.; Bayly, C. I.; Gould, I. R.; Merz, K. M.; Ferguson, D. M.; Spellmeyer, D. C.; Fox, T.; Caldwell, J. W.; Kollman, P. A. A second generation force field for the simulation of proteins, nucleic acids, and organic molecules. *J. Am. Chem. Soc.* **1995**, *117*, 5179–5197.
- URL: <http://amber.scripps.edu/doc6/amber6.pdf>.
- Lavery, R.; Sklenar, H. The definition of generalized helicoidal parameters and of axis curvature for irregular nucleic acids. *J. Biomol. Struct. Dyn.* **1988**, *6*, 63–91.
- De Lano, W., DeLano Scientific LLC. URL: <http://www.pymol.org/>.

JM060640Y